Title

E2/M1 mixing ratios in transitions from the gamma vibrational bands to the ground state rotational bands of 102, 104, 106, 108Mo, 108, 110, 112Ru, and 112, 114, 116Pd

Journal

The European Physical Journal A, 54(2)

ISSN

1434-6001

Authors

Eldridge, JM
Fenker, B
Hamilton, JH
et al.

Publication Date

2018-02-01

DOI

10.1140/epja/i2018-12426-5

Peer reviewed

Eur. Phys. J. A (2018) **54**: 15
DOI 10.1140/epja/i2018-12426-5

THE EUROPEAN PHYSICAL JOURNAL A

Regular Article – Experimental Physics

E2/M1 mixing ratios in transitions from the gamma vibrational bands to the ground state rotational bands of ^{102,104,106,108}Mo, ^{108,110,112}Ru, and ^{112,114,116}Pd*

J.M. Eldridge[1,a], B. Fenker[1,b], J.H. Hamilton[1], C. Goodin[1,c], C.J. Zachary[1], E. Wang[1], A.V. Ramayya[1], A.V. Daniel[2], G.M. Ter-Akopian[2], Yu.Ts. Oganessian[2], Y.X. Luo[1,3], J.O. Rasmussen[3], and S.J. Zhu[4]

[1] Department of Physics and Astronomy, Vanderbilt University, Nashville, TN 37240, USA
[2] Flerov Laboratory of Nuclear Reactions, JINR, Dubna, Russia
[3] Lawrence Berkeley National Laboratory, Berkeley, CA 94720, USA
[4] Department of Physics, Tsinghua University, Beijing 100084, China

Received: 3 October 2017
Published online: 19 February 2018 –
Communicated by T. Biro

Abstract. $E2/M1$ mixing ratios have been measured for transitions from states in the γ vibrational bands (I^+_γ) to states in the ground state bands (I^+ or $[I-1]^+$) of the neutron rich, even-even, deformed isotopes, ^{102,104,106,108}Mo, ^{108,110,112}Ru, and ^{112,114,116}Pd, including from states as high as 9^+_γ. These measurements were done using the GAMMASPHERE detector array, which, at the time of the experiment, had 101 working HPGe detectors, arranged at 64 different angles. A 62 μCi source of ^{252}Cf was placed inside GAMMASPHERE yielding 5.7×10^{11} γ-γ-γ and higher coincidence events. The angular correlations between the transitions from the γ-bands to the ground bands, and the pure $E2$ transitions within the ground band were then measured. These angular correlations yielded the mixing ratios, demonstrating that these transitions are pure or nearly pure $E2$, in agreement with theory. In order to correct for possible attenuation due to the lifetime of the intermediate state in these correlations, the g-factors of the intermediate states needed to be known. Therefore, the g-factors of the 2^+ states in the ground state band have been measured.

1 Introduction

The study of γ-rays emitted by an excited nucleus has long been a valuable tool in the study of nuclear structure. In particular the multipole mixing ratio of these γ-rays can give much information about the spin and parity of nuclear energy levels. When a nucleus decays from an excited state, the angular momentum selection rule for the emitted γ-ray is $|J_i - J_f| \leq L \leq J_i + J_f$. In practice, only the lowest two multipolarities are seen. Additionally, parity must be conserved in any electromagnetic nuclear decay producing additional selection rules. Electric radiation of multipolarity L has parity $\pi_e = (-1)^L$ while magnetic radiation has parity $\pi_m = (-1)^{L+1}$. Using these selection rules, a γ-decay from a 2^+ state into a 1^+ state permits $M1$, $E2$, or $M3$ radiation but only the $M1$ and $E2$ components are ever observed experimentally. Furthermore, electric multipole radiation is favored over its magnetic counterpart in deformed nuclei leading to $E(L+1)/ML$ mixtures but leaving $M(L+1)/EL$ mixtures extremely rare.

Because the γ vibrational band represents, in deformed nuclei, vibrations of a quadrupole state ($I^\pi = 2^+$), and subsequent rotations of that vibrational state, electromagnetic radiation emitted when a nucleus decays from the γ-band to the ground state rotational band is expected to be pure quadrupole [1]. Thus, only an $E2$ component should be observed in $\Delta I = 0, 1$, γ-band to ground band decays which would normally permit a $E2/M1$ mixing. Previous work by Goodin [2] has called this theory into question for some transitions in ^{102,104,106,108}Mo, ^{108,110,112}Ru, and ^{112,114,116}Pd. This work seeks to correct Goodin's measurements and confirm this prediction in these 10 isotopes, by γ-γ angular correlation.

* Contribution to the Topical Issue "Frontiers in Nuclear, Heavy Ion and Strong Field Physics" edited by Tamás S. Biró, Carsten Greiner, Berndt Müller, Johann Rafelski, Horst Stöcker.

[a] e-mail: jonathan.m.eldridge@gmail.com
[b] *Present address*: Physics Department, Texas A&M College Station, TX 77843, United States of America.
[c] *Present address:* Army Corp of Engineers, Waterways Experiment, Vicksburg, MS.

These mixing ratios, symbolized by $\delta(E2/M1)$ (or δ), are defined by

$$\delta^2(E2/M1; J_1 \to J_2) = \frac{T(E2; J_1 \to J_2)}{T(M1; J_1 \to J_2)}, \qquad (1)$$

where $T(E2)$ is the probability of an $E2$ transition, and J_1 is the spin of the higher level involved. The Krane-Steffen convention for the sign of the mixing ratio has been used in this work [3].

While the absolute sign of the mixing ratios is a matter of convention, a change in the sign from one nucleus to another can be indicative of a change in nuclear shape since the mixing ratio is proportional to the quadrupole operator. Krane [4] predicts that such a shape change should occur at around ^{110,112}Ru.

Greiner, in a 1966 paper [5] produced a theory exploring the consequences of differing proton and neutron deformation parameters, resulting from differing proton and neutron pairing forces. This theory allows one to calculate mixing ratios for primarily rotational nuclei by

$$\left(\frac{\delta}{E}\right)_{I_i \to I_f} = \left(8.6 \times 10^{-6} \frac{\beta_p^2 (1 - 0.72\beta_p)^2}{f^2(1-2f)^2} A^{\frac{10}{3}} \times \frac{\langle I_f 0, 22 | I_i 2\rangle^2}{\langle I_f 1, 11 | I_i 2\rangle^2} \frac{1}{I_f(I_f+1)}\right)^{1/2} \text{MeV}^{-1} \qquad (2)$$

and for $2^+_\gamma \to 2^+$ transitions in primarily vibrational nuclei

$$\left(\frac{\delta}{E}\right)_{2^+_\gamma \to 2^+} = 8.6 \times 10^{-4} \frac{A^{5/3}\beta_0}{(1-2f)f}, \qquad (3)$$

where f is a quadrupole correction factor defined by

$$f = \frac{\beta_2 - \beta_p}{\beta_2} = 1 - \frac{A}{N\frac{\beta_n}{\beta_p} + Z}. \qquad (4)$$

In these equations, β_2, β_p, and β_n are the nuclear, proton, and neutron quadrupole deformations, respectively, β_0 is an effective, or mean, deformation factor for a vibrating nucleus. In this work, we have made the simplifying assumption that $\beta_0 = \beta_2$. Greiner's theory implicitly depends upon the proton and neutron pairing forces, $G_p = 25/A$ and $G_n = 18/A$, respectively, where we have chosen to adopt values proposed by Nilsson and Prior [6]. It should be noted that Greiner's theory predicts all positive mixing ratios.

The gyromagnetic ratio, or g-factor, of a nuclear state is a dimensionless quantity which characterizes the magnetic properties of the nucleus in that state. A g-factor is defined by the ratio of the nuclear state's magnetic moment, $\boldsymbol{\mu}$, to its spin angular momentum, $\mathbf{I}$;

$$\boldsymbol{\mu} = g\frac{\mu_N}{\hbar}\mathbf{I}, \qquad (5)$$

where $\mu_N \equiv \frac{e\hbar}{2m_p}$ is the nuclear magneton. The g-factors of a nucleus's excited states can be used to determine many unique and interesting properties of the nucleus. Of particular interest in this work is the relationship between g and the angle, ϕ, through which the nucleus will rotate while in a particular state,

$$\phi = -B\tau g\frac{\mu_N}{\hbar}, \qquad (6)$$

where B is the external magnetic field and $\tau \equiv t_{1/2}/\ln 2$ is the lifetime of the nuclear state.

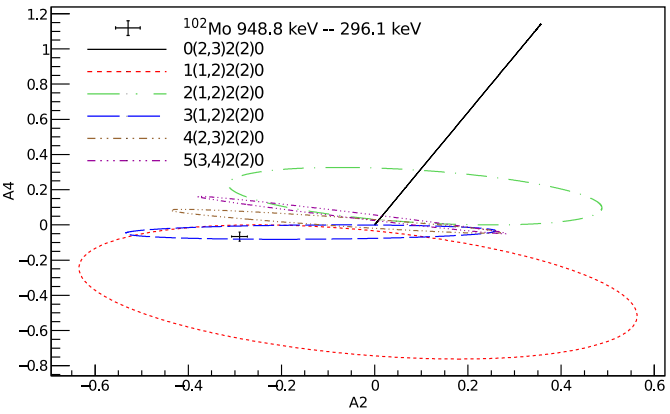

Fig. 1. Several examples of various δ ovals. These are compared to the 948.8 keV - 296.1 keV angular correlation from ^{102}Mo, demonstrating the confirmation of the spin of the 1244.9 keV level.

2 Experiment and methods

The experiment was conducted using the GAMMASPHERE detector array, which was at Lawrence Berkley National Laboratory at the time. A 62 μCi source of ^{252}Cf was placed between iron foils inside GAMMASPHERE yielding 5.7×10^{11} γ-γ-γ and higher coincidence events. Because the iron foils were thick enough to stop the fission fragments, no Doppler correction was needed on the measurements. At the time of the experiment, 101 of GAMMASPHERE's 110 Hyper-Pure Germanium (HPGe) γ-ray detectors were working. These detectors are arranged spherically about the source, with 64 possible angles between any two detectors. More details on this experimental setup can be found in Luo *et al.* [7].

The mixing ratios were measured by the Integral Perturbed Angular Correlation (IPAC) method, whereby the distribution of angles between two γ-rays in coincidence are fitted to

$$W(\theta) = 1 + G_2A_2P_2(\cos\theta) + G_4A_4P_4(\cos\theta), \qquad (7)$$

where P_l is a Legendre polynomial and G_k is a constant attenuation factor, to be discussed below. The parameters A_k can either be used as fit parameters or theoretically calculated as functions of the mixing ratios of the two γ-rays, δ_1 and δ_2, respectively. When one mixing ratio is held fixed, the theoretical values of A_2^{thry}, A_4^{thry} become a parametric equation which forms an oval as δ, starting at $-\infty$, comes back around to the same A_2^{thry}, A_4^{thry} at $\delta = +\infty$.

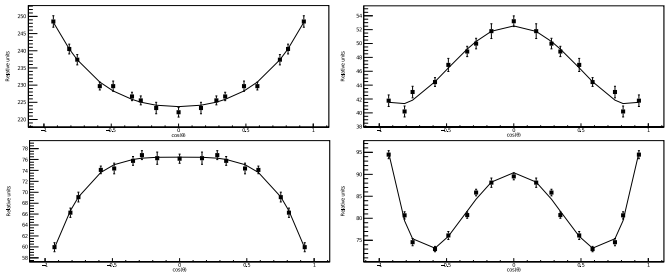

Fig. 2. Examples of angular correlation plots in this work. Top Left: the $4^+ \rightarrow 2^+ \rightarrow 0^+$ correlation from ^{104}Mo. Top Right: the $4^+_\gamma \rightarrow 4^+ \rightarrow 2^+$ correlation from ^{106}Mo. Bottom left: the $3^+_\gamma \rightarrow 2^+ \rightarrow 0^+$ correlation from ^{110}Ru. Bottom right: the $2^+_\gamma \rightarrow 2^+ \rightarrow 0^+$ correlation from ^{112}Pd.

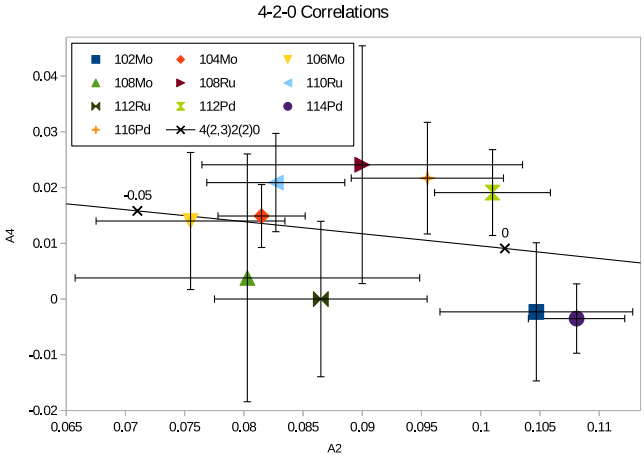

Fig. 3. A Plot of all the $4^+ \rightarrow 2^+ \rightarrow 0^+$ correlations measured in this work.

Figure 1 shows several examples of such a δ ovals compared to the results of one particular angular correlation. For details on how the A_k^{thry} parameters are calculated see Frauenfelder and Steffen [8]. Before the experimental results were fit to eq. (7), in order that there would be more statistics behind each data point, the 64 angular bins innate to GAMMASPHERE were combined to 17 angle bins, which were subsequently combined in pairs across the $\cos\theta = 0$ axis of symmetry to an effective 9 bins. Figure 2 shows examples of these angular correlations. Once A_2^{exp}, A_4^{exp} are thus measured, they are compared to the oval and the nearest A_2^{thry}, A_4^{thry}, falling exactly on the oval, and the corresponding value of δ is identified. Typically only A_2^{exp} was used in these calculations, since its uncertainty is usually smaller and small contaminations in the correlation affect A_4^{exp} to a greater extent. To aid in these calculations, the program DELTA, provided by the National Nuclear Data Center, was used [9].

Because IPAC depends on the angle between two γ-rays, any rotation the nucleus undergoes while in the intermediate nuclear state will attenuate the resultant angular correlation. If the attenuations factors, G_k, in eq. (7) are known, one can correct for this attenuation. G_k is defined as the ratio of the experimental and theoretical A_k factors

$$G_k \equiv \frac{A_k^{exp}}{A_k^{thry}} \,. \tag{8}$$

If, for a correlation whose unattenuated A_2^{thry}, A_4^{thry} we know, we can indirectly measure the angle through which the nucleus rotates, ϕ,

$$G_k = \frac{1}{2k+1}\left(1 + 2\sum_{q=1}^{k} \frac{1}{1+q^2\phi^2}\right). \tag{9}$$

Combining eqs. (6) and (9), we can use G_k to find the g-factor of an excited state. The g-factors of the 2^+ excited states of the nuclei discussed in this paper were measured using the $4^+ \rightarrow 2^+ \rightarrow 0^+$ angular correlation in each isotope. For these correlations, G_2 was found by eq. (8), and eqs. (9) and (6) were then solved for ϕ and g. These values of g and ϕ were then used in eq. (9) to find G_4. Since this method of calculating the g-factor depends on the difference between theoretical and experimental values of A_2, A_4, the uncertainty of the g-factor (and subsequently G_4) would be expected to increase as this difference decreases.

Often, multiple fission products of ^{252}Cf will have extremely similar energies in their cascades. This can be especially true for isotopes of the same element. Since IPAC is an essentially γ-γ coincidence method, we can take full advantage of the γ-γ-γ coincidence nature of our data to eliminate much of this source of background contamination by requiring that the cascades of interest be in coincidence with another γ-ray, either from the nuclide in question or from one of its fission partners. Our software is set up to allow us to select up to 10 such gates, requiring that the cascade of interest be in coincidence with *at least* one of them. More information on our implementation of IPAC (including corrections for differences in the individual detectors and the number of detectors in each angular bin) can be found in Daniel *et al.* [10] and Goodin [2].

3 Results

Results are presented here for the angular correlations measured and the corresponding g-factors and mixing ratios. These results have confirmed the spin assignment of the 1244.9 keV, $3^{(+)}_\gamma$ level in ^{102}Mo. The rest of the mixing ratios presented demonstrate that, as predicted, these transitions are nearly pure $E2$, and agree with Krane's [4] predicted shape transition. However, Greiner's [5] theory consistently under-predicts the values of $\delta(E2/M1)$ in this region. The errors given in this work for A_2^{exp}, A_4^{exp} are primarily statistical and represent 1 standard deviation (1σ). Considering how A_2, A_4 depend on δ, the uncertainty on values of δ measured represent 1σ in A_2, A_4 space, rather than on the δ number-line.

3.1 g-Factors and attenuation factors of 2^+ excited states

Figure 3 and table 1 display the results of the $4^+ \rightarrow 2^+ \rightarrow 0^+$ angular correlations measured for each of the

Table 1. Attenuation factors and g-factors of 2^+ excited states measured by $4^+ \rightarrow 2^+ \rightarrow 0^+$ angular correlations (theoretical $A_2, A_4 = 0.10204, 0.00907$). The Hyper-Fine Magnetic Fields experienced by each nuclide are taken from Rao [11]. For the Isotopes of Mo, $B = 25.6(5)$ T. For Ru, $B = 50.0(10)$ T. For Pd, $B = 54.7(38)$ T. The nuclear lifetimes, τ, are taken from refs. [12–19]. An uncertainty of ∞ indicates that the parameter could not be determined with any reasonable precision. The symbol * indicates that this additional gate is from a fission partner.

Nuclide	Additional gates	A_2^{exp}, A_4^{exp}	τ (ns)	G_2, G_4	g-factor
^{102}Mo	584, 691, 181*	0.105(8), 0.00(2)	0.180(6)	1.03(8), 0.9(7)	0.8(6)
^{104}Mo	519, 642, 734, 800, 860	0.082(4), 0.015(6)	1.40(12)	0.80(4), 0.6(1)	0.22(3)
^{106}Mo	655	0.076(8), 0.01(1)	1.80(4)	0.74(8), 0.5(1)	0.21(5)
^{108}Mo	527, 662, 415	0.08(1), 0.00(2)	0.7(4)	0.8(1), 0.6(5)	0.5(2)
Average for $^{104-108}$Mo: $G_2, G_4 = 0.78(6), 0.6(2)$					
^{108}Ru	1446, 798, 518, 163, 443, 1232	0.09(1), 0.02(2)	0.52(4)	0.9(1), 0.7(7)	0.2(2)
^{110}Ru	705, 815	0.083(6), 0.021(9)	0.46(3)	0.81(6), 0.6(1)	0.34(7)
^{112}Ru	589*, 484*, 400*, 723, 1220*	0.087(9), 0.00(1)	0.46(4)	0.85(9), 0.7(3)	0.3(1)
Average for $^{108-112}$Ru: $G_2, G_4 = 0.85(6), 0.7(2)$					
^{112}Pd	None	0.101(5), 0.019(8)	0.121(20)	0.99(5), 1(2)	0.2(6)
^{114}Pd	648, 716, 644, 584	0.108(4), −0.004(6)	0.118(20)	1.06(4), 1(∞)	0(∞)
^{116}Pd	None	0.096(6), 0.02(1)	0.16(4)	0.94(6), 0.9(5)	0.5(3)
$G_2 = G_4 = 1$ used for ^{102}Mo and ^{112,114,116}Pd					

10 nuclides considered in this work. According to theory, these angular correlations should all fall at the point $A_2, A_4 = 0.10204, 0.00907$, which corresponds to $0 = \delta_1(M3/E2) = \delta_2(M3/E2)$. The primary purpose of these correlations, as described in sect. 2, was to correct for any attenuation caused by the lifetime of the 2^+ states. Table 1 shows the results of these correlations. For ^{102}Mo and ^{112,114,116}Pd, the attenuation factors, G_2, G_4, were determined to be close enough to 1 that no correction was used for these nuclides. The values for the attenuation factors for ^{104,106,108}Mo and for ^{108,110,112}Ru were averaged, to reduce uncertainties. For these isotopes of Mo it was determined that $G_2, G_4 = 0.78(6), 0.6(2)$, while for the isotopes of Ru, $G_2, G_4 = 0.85(6), 0.7(2)$. These averages were used to correct the $2^+_\gamma \rightarrow 2^+ \rightarrow 0^+$ and $3^+_\gamma \rightarrow 2^+ \rightarrow 0^+$ correlations for these isotopes. It is assumed that the lifetimes of 4^+ and higher states are short enough that there is no attenuation.

The g-factors measured in this work generally agree with those cited in Chamoli *et al.* [20], and two papers by Smith *et al.* [21,22], though the uncertainties in the present work are generally larger than those cited in these previous works. Of particular note, however, is the g-factor for ^{112}Pd, for which, though its uncertainty is extremely large, no value for it has been previously reported in the literature.

3.2 Mixing ratios of γ-band to Yrast-band transitions

Tables 2, 3, and 4 contain information about the angular correlations measured and the subsequent calculations of mixing ratios for γ-band to ground state band transitions measured in this work. Typically, these calculations of δ used only A_2. Because possible values of δ make an oval in A_2, A_4 space, a given value of A_2 will usually have two possible values of A_4 (and vice versa), corresponding to two different values of δ. In these three tables all possible solutions within 3σ of A_2^{exp}, A_4^{exp} have been given, but those solutions which are also greater than 1.5σ have been marked off with square braces. The measured $2^+_\gamma \rightarrow 2^+ \rightarrow 0^+$ correlations, $3^+_\gamma \rightarrow 2^+ \rightarrow 0^+$ correlations, $4^+_\gamma \rightarrow 4^+ \rightarrow 4^+$ correlations, and $5^+_\gamma \rightarrow 4^+ \rightarrow 2^+$ correlations can be seen compared to the appropriate respective δ ovals in figs. 4, 5, 6, and 7, respectively.

3.2.1 Isotopes of Mo

Table 2 lists all the angular correlation measurements for γ-band to Yrast-band transitions that were feasible in our data for ^{102,104,106,108}Mo. The complete level scheme of ^{102}Mo, as considered in this work is found in Yang *et al.* [23]. For ^{104}Mo and ^{106}Mo see Jones *et al.* [24]. For ^{108}Mo see Ding *et al.* [25]. Select correlations for the four isotopes of Mo considered are shown in fig. 8.

In ^{102}Mo, the present work has confirmed the assignments of Yang *et al.* [23], that the band with the 2^+, 847.5 keV band-head is the one phonon γ-band for ^{102}Mo and their assignment of the 1244.9, (3^+) level to this band. Figure 1 compares the result of this correlation to the δ ovals corresponding to each of the possible spins for this level from 0 to 5. Clearly only the $3(1,2)2(2)0$ oval matches the results of the correlation, thus we firmly assign a spin of 3 to the 1244.9 level.

Table 2. Table of delta values measured in this work for the isotopes of Mo. A_2^{raw}, A_4^{raw} refer to the raw A_2^{exp}, A_4^{exp} fit values, while A_2^{cor}, A_4^{cor} refer to the values of A_2^{exp}, A_4^{exp} which have been corrected for attenuation according to table 1. Often two solutions are warranted for δ, given A_2^{exp}, A_4^{exp} within 3σ. Square braces, "[ ]", indicate that A_2^{thry} (or A_4^{thry}) differs from A_2^{exp} (A_4^{exp}) by more than 1.5σ.

Transition	Additional gates	A_2^{raw}, A_4^{raw}	A_2^{cor}, A_4^{cor}	δ	A_2^{thry}, A_4^{thry}
		^{102}Mo			
$2_\gamma^+ \rightarrow 2^+$	1633, 551, 397, 331*, 611, 200*, 367	−0.17(1), 0.31(2)	–	$7.0^{+1.8}_{-0.6}$	−0.173, 0.320
$3_\gamma^+ \rightarrow 2^+$	1235, 624, 1200, 333*, 1376, 182*, 445*, 752	−0.29(3), −0.07(3)	–	-9^{+2}_{-3} [−0.28(2)]	−0.289, −0.081 −0.286, [−0.006]
$4_\gamma^+ \rightarrow 4^+$	296, 1082, 181*, 333*, 1223, 200*, 1265, 431*	−0.18(2), 0.13(3)	–	2^{+3}_{-1}	−0.179, 0.131
		^{104}Mo			
$2_\gamma^+ \rightarrow 2^+$	771, 478, 331*, 200*, 432*, 509*, 241, 343*, 403, 216	−0.12(2), 0.23(3)	−0.15(3), 0.4(1)	9^{+4}_{-2} [0.60(4)]	−0.156, 0.322 −0.160, [0.087]
$3_\gamma^+ \rightarrow 2^+$	556, 200*, 478, 331*	−0.146(9), −0.07(1)	−0.19(2), −0.12(4)	$50^{+\infty}_{-27}$ [−0.15(2)]	−0.189, −0.082 −0.188, [−0.002]
$4_\gamma^+ \rightarrow 4^+$	192, 510, 331*, 200*, 432*, 369*, 478, 113*, 118*, 260	−0.16(1), 0.16(2)	–	7^{+3}_{-1}	−0.156, 0.158
$5_\gamma^+ \rightarrow 4^+$	192, 561, 646, 200*	−0.10(1), −0.6(2)	–	30^{+16}_{-8}	−0.105, −0.059
$7_\gamma^+ \rightarrow 6^+$	192, 387, 646, 714, 200*, 331*, 431*, 118*	−0.01(3), 0.07(5)	–	0.10(4) [7^{+3}_{-1}]	−0.007, −0.001 −0.007, [−0.050]
$9_\gamma^+ \rightarrow 8^+$	192, 369, 519, 200*, 331*, 118*, 113*, 432*, 713, 165*	0.10(6), −0.15(9)	–	3(1) [$0.31^{+0.10}_{-0.09}$]	0.102, −0.043 0.102, [−0.004]
		^{106}Mo			
$2_\gamma^+ \rightarrow 2^+$	724, 360*	−0.18(2), 0.27(8)	−0.18(2), 0.27(8)	$6.2^{+1.0}_{-0.8}$ [0.65(5)]	−0.184, 0.318 −0.180, [0.096]
$3_\gamma^+ \rightarrow 2^+$	422, 1052, 773, 550	−0.058(8), −0.05(1)	−0.08(1), −0.08(3)	$6.1^{+0.7}_{-0.6}$ [−0.01(2)]	−0.075, −0.079 −0.075, [0.000]
$4_\gamma^+ \rightarrow 4^+$	172, 496	−0.19(1), 0.11(2)	–	[$2.1^{+0.6}_{-0.4}$]	[−0.177], 0.123†
$5_\gamma^+ \rightarrow 4^+$	172, 561, 784, 200*, 360*	0.023(7), −0.05(1)	–	4.4(2)	0.023, −0.056
$6_\gamma^+ \rightarrow 6^+$	172, 351	−0.07(2), 0.04(3)	–	1.1(1) [-5^{+1}_{-2}]	−0.075, 0.061 −0.075, [0.108]
$7_\gamma^+ \rightarrow 6^+$	none	0.08(3), −0.08(5)	–	$3.2^{+0.8}_{-0.6}$ $0.26^{+0.06}_{-0.05}$	0.080, −0.047 0.080, −0.003
		^{108}Mo			
$2_\gamma^+ \rightarrow 2^+$	393	−0.08(3), 0.19(5)	−0.11(5), 0.3(1)	$23^{+\infty}_{-14}$ [0.50(6)]	−0.107, 0.326 −0.107, [0.065]
$3_\gamma^+ \rightarrow 2^+$	449, 585, 916, 639, 707, 725, 1047, 1129, 991, 1092	−0.12(2), −0.03(4)	−0.15(4), −0.05(7)	15^{+33}_{-6} −0.10(4)	−0.150, −0.081 −0.150, −0.001
$4_\gamma^+ \rightarrow 4^+$	530, 589*, 602*, 662, 658*, 254, 720, 779, 979	0.00(4), −0.01(7)	–	1.1(2) $\infty(^{>+50}_{<-75})^\ddagger$	−0.119, 0.080 −0.118, 0.152

* Indicates that this additional gate is from a fission partner.

† For this measurement, δ was calculated using both A_2^{exp} and A_4^{exp}, rather than only A_2^{exp}.

‡ This solution is exactly pure $E2$ ($\delta = \pm\infty$). In parentheses are values allowed within 1σ.

Table 3. Table of delta values measured in this work for the isotopes of Ru. A_2^{raw}, A_4^{raw} refer to the raw A_2^{exp}, A_4^{exp} fit values, while A_2^{cor}, A_4^{cor} refer to the values of A_2^{exp}, A_4^{exp} which have been corrected for attenuation according to table 1. Often two solutions are warranted for δ, given A_2^{exp}, A_4^{exp} within 3σ. Square braces, "[ ]", indicate that A_2^{thry} (or A_4^{thry}) differs from A_2^{exp} (A_4^{exp}) by more than 1.5σ.

Transition	Additional gates	A_2^{raw}, A_4^{raw}	A_2^{cor}, A_4^{cor}	δ	A_2^{thry}, A_4^{thry}
		^{108}Ru			
$2_\gamma^+ \to 2^+$	none	−0.10(1), 0.21(2)	−0.12(2), 0.3(1)	16^{+9}_{-4} $[0.52^{+0.03}_{-0.02}]$	−0.120, 0.325 −0.120, [0.070]
$3_\gamma^+ \to 2^+$	521, 851, 637, 669, 182, 711, 200, 726, 443, 771	−0.20(2), −0.06(4)	−0.23(3), −0.09(6)	$-28^{+20}_{-\infty}$ −0.21(3)	−0.232, −0.082 −0.234, −0.003
$4_\gamma^+ \to 4^+$	243, 377*, 579, 458*, 439*, 572*, 583*, 589*, 585*, 77*	−0.20(2), 0.08(4)	–	$1.8^{+0.9}_{-0.4}$	−0.172, 0.117†
		^{110}Ru			
$2_\gamma^+ \to 2^+$	472, 600, 247, 713, 516, 291	−0.07(1), 0.22(2)	−0.08(2), 0.3(1)	$\infty(^{>+50}_{<-75})^\ddagger$ [0.45(2)]	−0.077, 0.327 −0.079, [0.055]
$3_\gamma^+ \to 2^+$	516, 646, 868, 395	−0.175(8), −0.07(1)	−0.21(2), −0.11(4)	$\infty(^{>+55}_{<-41})^\ddagger$ [0.45(2)]	−0.204, −0.082 −0.206, [−0.002]
$4_\gamma^+ \to 4^+$	600, 713, 291, 932	−0.15(3), 0.13(5)	–	7^{+96}_{-6}	−0.154, 0.149
$5_\gamma^+ \to 4^+$	646, 756, 868, 395	−0.10(2), 0.01(3)	–	−0.04(2) $[22^{+28}_{-8}]$	−0.096, 0.000 −0.096, [−0.059]
		^{112}Ru			
$2_\gamma^+ \to 2^+$	457, 224, 589	−0.04(1), 0.18(2)	−0.05(1), 0.3(1)	-30^{+10}_{-31} [0.41(2)]	−0.052, 0.326 −0.052, [0.046]
$3_\gamma^+ \to 2^+$	488, 606, 694	−0.16(1), −0.08(2)	−0.19(2), −0.12(5)	$43^{+\infty}_{-22}$ [−0.15(3)]	−0.186, −0.082 −0.186, [−0.002]

* Indicates that this additional gate is from a fission partner.
† For this measurement, δ was calculated using both A_2^{exp} and A_4^{exp}, rather than only A_2^{exp}.
‡ This solution is exactly pure $E2$ ($\delta = \pm\infty$). In parentheses are values allowed within 1σ.

Often the uncertainty in A_2, A_4 space will include the point where $\delta = \pm\infty$. This is usually signified by an error of $+\infty$ on positive values or $-\infty$ on negative values, and means that pure $E2$ as well as both positive and negative values of δ are within 1σ in A_2, A_4 space. One of the solutions for the $3_\gamma^+ \to 2^+$ mixing ratio for ^{104}Mo is $\delta = 50^{+\infty}_{-27}$, indicating that the transition is indistinguishable from pure $E2$ and values of $\delta < -159$ are also allowed within 1σ of A_2^{exp}, A_4^{exp}. For ^{108}Mo, one solution lies at $\delta = 23^{+\infty}_{-14}$. In this case, in addition to indicating that pure $E2$ lies within 1σ, the $+\infty$ uncertainty indicates that values of $\delta < -51$ are allowed within 1σ in A_2, A_4 space.

Amongst the isotopes of Mo there were a few places where similarities in energy between various nuclides set limits on which extra gates could be chosen. The $2^+ \to 0^+$, 296.1 keV, transition in ^{102}Mo is close in energy to the $4^+ \to 2^+$, 295.2 keV transition in ^{148}Ce. For the $2_\gamma^+ \to 2^+ \to 0^+$ cascade for ^{102}Mo, the 401.1 keV γ-ray was not used as an additional gate, even though it is the second strongest peak in the coincidence spectrum, because it is also expected to be in coincidence with the $4^+ \to 2^+$, 295.2 keV γ-ray of ^{148}Ce. Additionally, the $3_\gamma^+ \to 2^+$ transition in ^{102}Mo has energy of 948.8 keV, while the $7_\gamma^+ \to 6^+$ transition in ^{148}Ce has energy, 948.9 keV. This meant that each additional gate used in the $3_\gamma^+ \to 2^+ \to 0^+$ needed to be carefully inspected to insure that it is not also found in ^{148}Ce nor an isotope of its fission partner, Zr.

The other major such complication for the isotopes of Mo was the similarity in energies between the $4_\gamma^+ \to 2_\gamma^+$, 392.5 keV and the $2_\gamma^+ \to 2^+$, 393.0 keV transitions of ^{108}Mo. This primarily caused trouble in measuring the $2_\gamma^+ \to 2^+ \to 0^+$ angular correlation. Several different extra gate combinations were tried to remove this contamination. Ultimately it was determined that using only the $4_\gamma^+ \to 2_\gamma^+$ itself produced the least attenuated and clearest correlation.

Table 4. Table of delta values measured in this work for the isotopes of Pd. Because, as shown in table 1, no correction for attenuation was needed for the isotopes of Pd, only one column is given for A_2^{exp}, A_4^{exp} (rather than splitting it into A_2^{raw}, A_4^{raw} and A_2^{cor}, A_4^{cor}). Often two solutions are warranted for δ, given A_2^{exp}, A_4^{exp} within 3σ. Square braces, "[ ]", indicate that A_2^{thry} (or A_4^{thry}) differs from A_2^{exp} (A_4^{exp}) by more than 1.5σ.

Transition	Additional gates	A_2^{exp}, A_4^{exp}	δ	A_2^{thry}, A_4^{thry}
		^{112}Pd		
$2_\gamma^+ \rightarrow 2^+$	360	0.020(6), 0.31(1)	$-7.9^{+0.3}_{-0.4}$	0.019, 0.321
$3_\gamma^+ \rightarrow 2^+$	560, 1099, 663, 1659, 353*	−0.45(1), −0.084(9)	−2.6(1)	−0.451, −0.071
$4_\gamma^+ \rightarrow 4^+$	349, 641, 424*, 353*	−0.08(3), 0.13(5)	$-8^{+\ 4}_{-47}$ 0.8(1)	−0.079, 0.150 −0.079, 0.062
$5_\gamma^+ \rightarrow 4^+$	none	−0.17(5), 0.06(8)	−0.15(6) $-18^{+\ 8}_{-81}$	−0.171, −0.001 −0.164, −0.059
		^{114}Pd		
$2_\gamma^+ \rightarrow 2^+$	317, 619, 626	−0.046(7), 0.30(1)	$[-25^{+3}_{-2}]$	−0.047, [0.326]
$3_\gamma^+ \rightarrow 2^+$	none	−0.37(1), −0.08(1)	−4.2(3)	−0.372, −0.077
$4_\gamma^+ \rightarrow 4^+$	333, 664	−0.17(5), 0.15(7)	$4^{+40}_{-\ 3}$	−0.168, 0.144†
$5_\gamma^+ \rightarrow 4^+$	333, 660, 1279*, 993, 297*, 890, 325*, 1509, 1151*	−0.16(7), −0.1(1)	$-21^{+11}_{-\infty}$ −0.13(8)	−0.160, −0.059 −0.158, −0.001
		^{116}Pd		
$2_\gamma^+ \rightarrow 2^+$	328, 636, 652, 744, 466	−0.06(1), 0.33(2)	$-74^{+\ 38}_{-282}$	−0.067, 0.326
$3_\gamma^+ \rightarrow 2^+$	652, 744, 466, 549, 774, 1151*, 1279*	−0.25(2), −0.09(3)	-15^{+3}_{-5}	−0.255, −0.081

* Indicates that this additional gate is from a fission partner.
† For this measurement, δ was calculated using both A_2^{exp} and A_4^{exp}, rather than only A_2^{exp}.

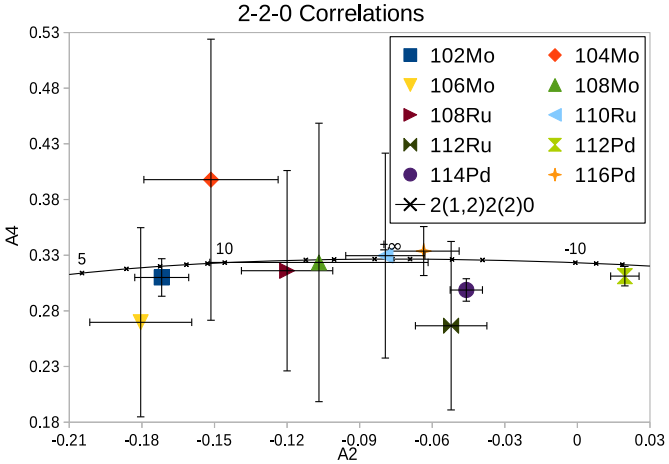

Fig. 4. A plot of all the $2_\gamma^+ \rightarrow 2^+ \rightarrow 0^+$ correlations measured in this work compared to the $2(1,2)2(2)0$ δ oval.

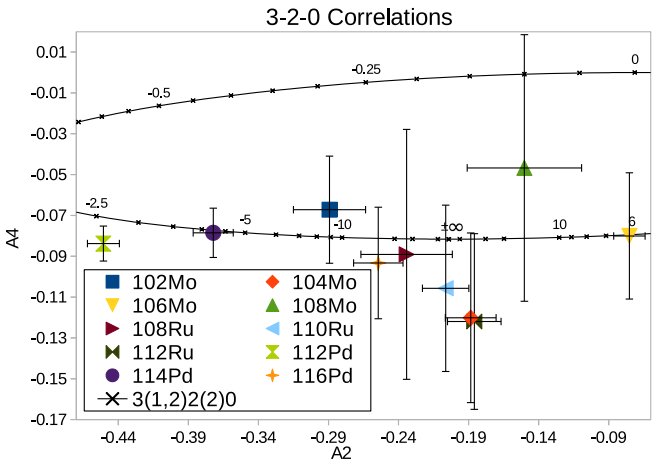

Fig. 5. A plot of all the $3_\gamma^+ \rightarrow 2^+ \rightarrow 0^+$ correlations measured in this work compared to the $3(1,2)2(2)0$ δ oval.

3.2.2 Isotopes of Ru

The complete level schemes for the isotopes of Ru considered in this work can be found in Luo *et al.* [26] and Zhu *et al.* [27]. Table 3 gives all the angular correlations and subsequent mixing ratios measured for these isotopes. Select correlations for the three isotopes of Ru considered are shown in fig. 9.

The first few transitions in the Yrast Bands of ^{108}Ru and ^{110}Ru are extremely similar. This caused difficulty measuring the $4^+ \rightarrow 2^+ \rightarrow 0^+$ transitions for these two isotopes. Only transitions seen in one isotope, but not the

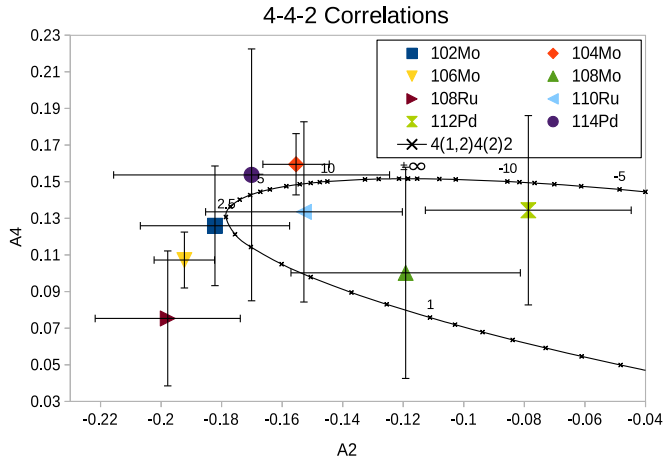

Fig. 6. A plot of all the $4^+_\gamma \rightarrow 4^+ \rightarrow 2^+$ correlations measured in this work compared to the $4(1,2)4(2)2$ δ oval.

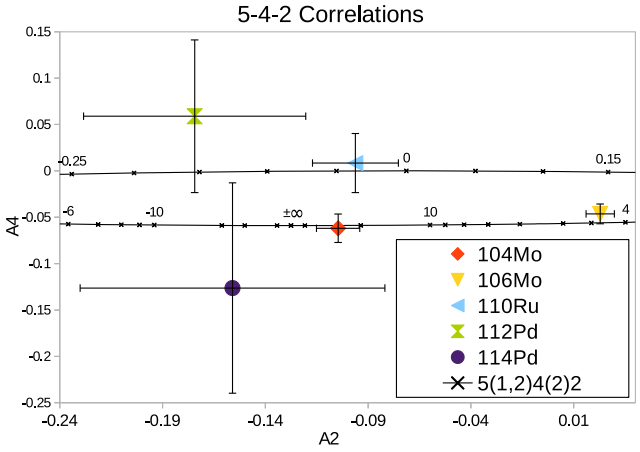

Fig. 7. A plot of all the $5^+_\gamma \rightarrow 4^+ \rightarrow 2^+$ correlations measured in this work compared to the $5(1,2)4(2)2$ δ oval.

other, were chosen as additional gates to ensure that the correlation measured was actually that of the desired isotope. However, the γ bands of these two isotopes are different enough that the similarities in the Yrast-band transitions caused little issue.

The $5^+_\gamma \rightarrow 4^+ \rightarrow 2^+$, 711.9 keV - 422.6 correlation for ^{110}Ru was the only other major such issue. This is primarily due to its proximity in energy to the $9^+_\gamma \rightarrow 7^+_\gamma$, 710.4 keV and $4^+ \rightarrow 2^+$, 422.9 keV transitions from ^{108}Ru, and its own $8^+_\gamma \rightarrow 6^+_\gamma$, 712.7 keV transition. After trying a number of additional combinations to weed out these sources of contamination, the four known transitions from ^{110}Ru found in coincidence with its $5^+_\gamma \rightarrow 4^+ \rightarrow 2^+$, but not its $8^+_\gamma \rightarrow 6^+_\gamma$ were deemed to produce the clearest and least attenuated correlation.

A value of $\delta(E2/M1) = -28^{+20}_{-\infty}$ is assigned as one of the solutions for the mixing ratio for the $3^+_\gamma \rightarrow 2^+$ transition in ^{108}Ru. In this case, the uncertainty of $-\infty$ indicates that the transition is indistinguishable from pure

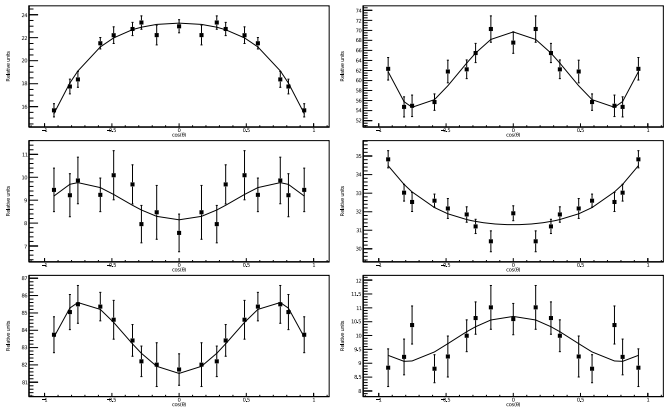

Fig. 8. Sample angular correlations for isotopes of Mo. Top left: the $3^+_\gamma \rightarrow 2^+ \rightarrow 0^+$ correlation for ^{102}Mo. Top right: the $2^+_\gamma \rightarrow 2^+ \rightarrow 0^+$ correlation for ^{104}Mo. Middle left: the $9^+_\gamma \rightarrow 8^+ \rightarrow 6^+$ correlation for ^{104}Mo. Middle right: the $4^+ \rightarrow 2^+ \rightarrow 0^+$ correlation for ^{106}Mo. Bottom left: the $5^+_\gamma \rightarrow 4^+ \rightarrow 2^+$ correlation for ^{106}Mo. Bottom right: the $4^+_\gamma \rightarrow 4^+ \rightarrow 2^+$ correlation for ^{108}Mo.

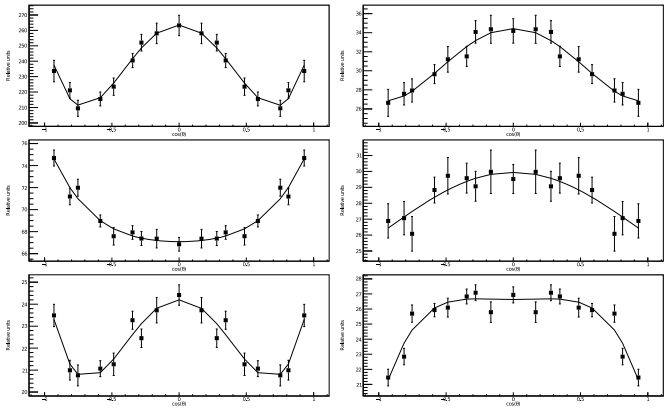

Fig. 9. Sample angular correlations for isotopes of Ru. Top left: the $2^+_\gamma \rightarrow 2^+ \rightarrow 0^+$ correlation for ^{108}Ru. Top right: the $4^+_\gamma \rightarrow 4^+ \rightarrow 2^+$ correlation for ^{108}Ru. Middle left: the $4^+ \rightarrow 2^+ \rightarrow 0^+$ correlation for ^{110}Ru. Middle right: the $5^+_\gamma \rightarrow 4^+ \rightarrow 2^+$ correlation for ^{110}Ru. Bottom left: the $2^+_\gamma \rightarrow 2^+ \rightarrow 0^+$ correlation for ^{112}Ru. Bottom right: the $3^+_\gamma \rightarrow 2^+ \rightarrow 0^+$ correlation for ^{112}Ru.

$E2$ and that values of $\delta(E2/M1) > 383$ are also allowed within 1σ of A_2^{exp}, A_4^{exp}. Similarly, one of the solutions for the $3^+_\gamma \rightarrow 2^+$ transition in ^{112}Ru is $\delta = 43^{+\infty}_{-22}$, indicating that, within 1σ of A_2^{exp}, A_4^{exp}, the transition is indistinguishable from pure $E2$ and values of $\delta < -816$ are allowed.

For ^{110}Ru the best solution was $\delta = \pm\infty$, or pure $E2$, for both the $2^+_\gamma \rightarrow 2^+$ and $3^+_\gamma \rightarrow 2^+$ transitions. The uncertainty on the $2^+_\gamma \rightarrow 2^+$ transition allows positive values of $\delta > 50$ and negative values < -75. For the $3^+_\gamma \rightarrow 2^+$ transition values of $\delta < -46$ and > 55 were within 1σ in A_2, A_4 space.

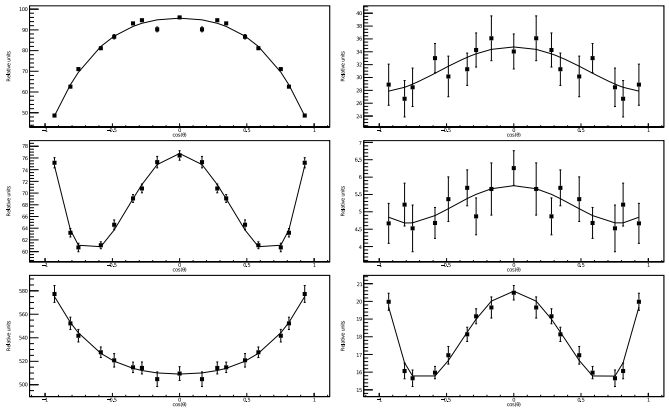

Fig. 10. Sample angular correlations for isotopes of Pd. Top left: the $3^+_\gamma \rightarrow 2^+ \rightarrow 0^+$ correlation for ^{112}Pd. Top right: the $5^+_\gamma \rightarrow 4^+ \rightarrow 2^+$ correlation for ^{112}Pd. Middle left: the $2^+_\gamma \rightarrow 2^+ \rightarrow 0^+$ correlation for ^{114}Pd. Middle right: the $4^+_\gamma \rightarrow 4^+ \rightarrow 2^+$ correlation for ^{114}Pd. Bottom left: the $4^+ \rightarrow 2^+ \rightarrow 0^+$ correlation for ^{116}Pd. Bottom right: the $2^+_\gamma \rightarrow 2^+ \rightarrow 0^+$ correlation for ^{116}Pd.

3.2.3 Isotopes of Pd

No major sources of commonalities between the transition energies of interest and transition energies from other nuclides were found. This lack of contamination and the lack of need for corrections for attenuation (see table 1) combined to cause the uncertainties for the isotopes of Pd to be generally lower than their counterpart measurements in either Mo or Ru. Another consequence was that measuring mixing ratios of transitions from higher spin states were possible for the isotopes of Pd than for those of Ru, even though the isotopes of Ru are more frequently produced in the Spontaneous fission of ^{252}Cf.

The complete level schemes of ^{112,114,116}Pd, as considered in this work, can be found in Luo *et al.* [28]. Table 4 gives all the angular correlations and subsequent mixing ratios measured for these isotopes. Select correlations for the three isotopes of Pd considered are shown in fig. 10.

For the mixing ratio of the $5^+_\gamma \rightarrow 4^+$ transition in ^{114}Pd a value of $\delta = -20^{+11}_{-\infty}$ has been assigned. The $-\infty$ uncertainty indicates that the transition is indistinguishable from pure $E2$ and that positive values, > 15 are also allowed for this mixing ratio within 1σ in A_2^{exp}, A_4^{exp} space.

4 Discussion

One can see, looking at tables 2, 3, 4, and fig. 11 that 30 of the 37 mixing ratios ($\sim$ 81%) measured demonstrate a pure or near-pure $E2$ transition (namely, $|\delta| \geq 3 \rightarrow \%E2 \geq 90\%$) within 1.5σ in A_2, A_4 space. Noting that the uncertainties in tables 2, 3, and 4 for values of δ represent 1σ in A_2, A_4 space, all of the 37 mixing ratios measured can be pure or near-pure $E2$ within 3σ. However, these results are lower than the simpler theory that states, based on the quadrupole nature of the 2^+_γ state, that these transitions should all be pure or nearly pure $E2$. This simplistic theory's prediction would be based primarily on statistical distributions, stating that 87% of the data (or $\sim$ 32 of 37) should be pure or nearly pure $E2$ within 1.5σ and ~ 36.8 of 37 would be pure or nearly pure $E2$ within 3σ. Since the sample size here is small, it is likely that this fluctuation is random and would be resolved were more mixing ratios measured, especially since the choice of $|\delta| \geq 3$ as the benchmark is relatively arbitrary. Thus we conclude that, from a statistical standpoint, all of the mixing ratios measured in this work are pure or nearly pure $E2$, in accordance with theory.

Greiner's theory [5], detailed in eqs. (2) through (4), however, makes much more precise predictions of these mixing ratios than simply that they should be pure or nearly pure $E2$. Equations (2) through (4) are plotted alongside the experimental mixing ratios measured in this work in fig. 11. Since many of the variables in Greiner's theory are only known through experiment, appropriate 1σ uncertainties have been included in the theory. Most of the experimental variables required were found in refs. [12–19]. Because Greiner's theory does not predict any sign changes in the mixing ratios, both the positive and negative of it have been plotted. As can be seen in fig. 11, Greiner's theory consistently under-predicts the magnitude of the mixing ratios except for the $3^+_\gamma \rightarrow 2^+$ mixing ratio for ^{112}Pd, which is probably random, and the $4^+_\gamma \rightarrow 4^+$ mixing ratios, which generally have larger uncertainties. Thus Greiner's theory is not accurate for this section of the chart of nuclides.

Krane [4] predicted that there would be a shape change in nuclei at around ^{110}Ru which would correspond to a change in the relative sign in the mixing ratios of γ-band to ground band transitions. This has been clearly observed, especially in the $2^+_\gamma \rightarrow 2^+$ transitions as seen in fig. 11. Additionally, there is a generally increasing trend among the $2^+_\gamma \rightarrow 2^+$ mixing ratios for Mo and Ru, where for Ru the trend crosses $\pm\infty$ at ^{110}Ru and continues in negative numbers (*i.e.*, a decreasing trend in $1/\delta$). The Pd isotopes, however, show a decreasing trend, but are all negative. In general, the higher order mixing ratios confirm these trends, though not quite as clearly.

5 Conclusion

The mixing ratios have been measured for γ-band to ground band transitions which would normally allow sizable $E2/M1$ mixing in ^{102,104,106,108}Mo, ^{108,110,112}Ru, and ^{112,114,116}Pd. The 37 mixing ratios have been found to be greater than 90% $E2$, within 3 standard deviations, very nearly modeling statistical expectations based on the fact that the 2^+_γ state is a quadrupole state. However, Greiner's theory consistently under-predicted the values of thes mixing ratios. Based on these mixing ratios, we have observed

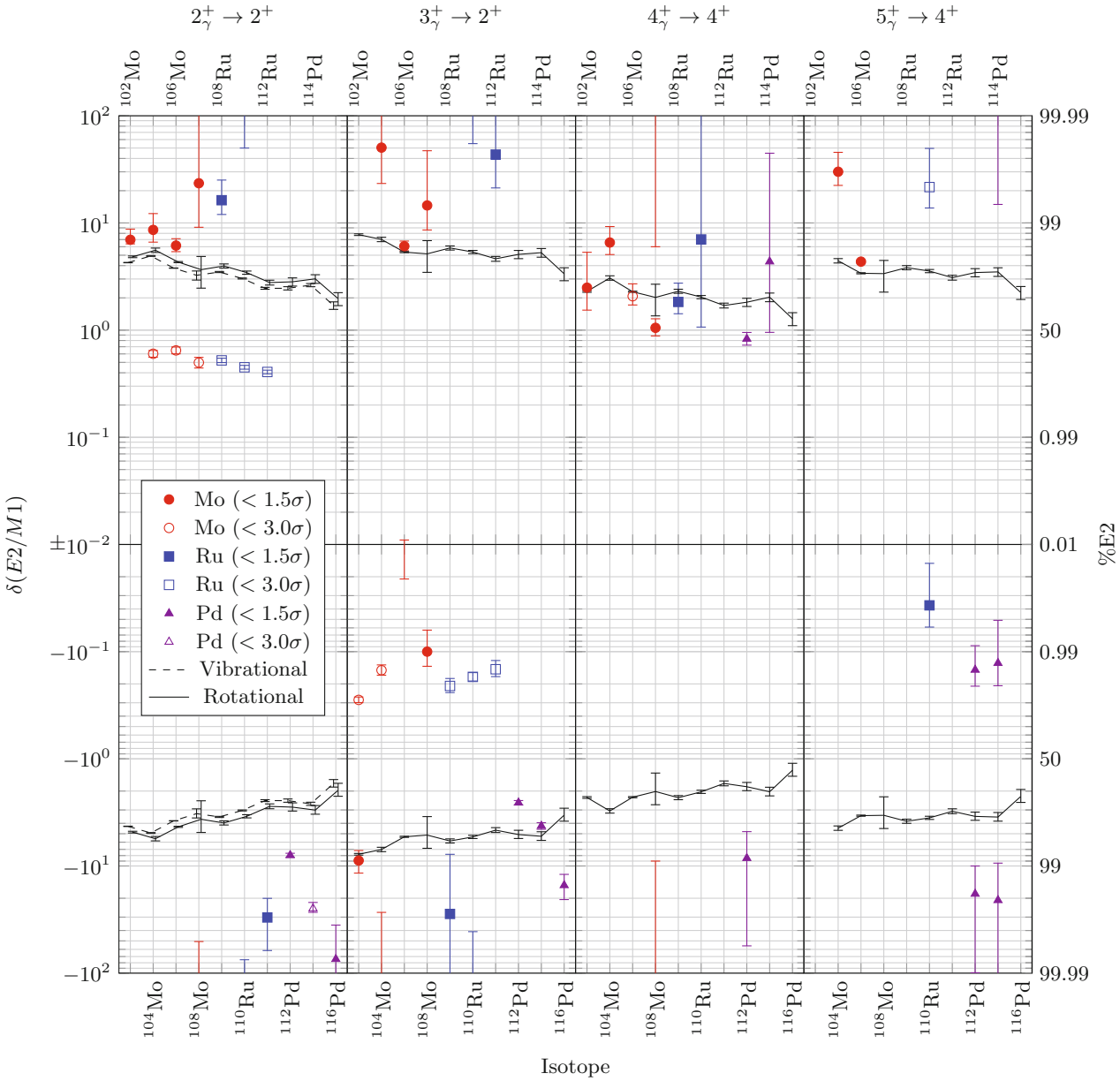

Fig. 11. Plots of mixing ratios measured in this work compared with Greiner's rotational and vibrational theories [5], given in eqs. (2) and (3), respectively. Greiner's two theories are plotted as black solid and dashed lines, respectively, with 1σ uncertainty. Since Greiner's theory predicts all positive values for δ, the negative of his theory has also been given. These data are plotted on a positive and negative log scale from $\pm 10^{-2}$ to $\pm 10^{2}$. Each column contains the mixing ratios for a particular transition for all isotopes. Mixing ratios less than 1.5σ in the uncertainty of both A_2^{exp} and A_4^{exp} are given with filled in points, while those which are between 1.5 and 3.0σ in either A_2^{exp} or A_4^{exp} are hollow. The mixing ratios whose value was determined to be $\pm\infty$ do not appear on the graph, but the lower bound on positive numbers and upper bound on negative numbers can be seen. In a similar manner, mixing ratios whose values overlap with $\delta = \pm\infty$, show uncertainty which wraps around the graph.

the predicted shape change around ^{110}Ru. We have confirmed the assignment of a 1244.9 keV level in ^{102}Mo as the 3^+ level in its one phonon γ-band. The g-factors of the first 2^+ excited states of these nuclides have been measured and are consistent with previous measurements. Further work needs to be done to determine if the trends observed in the mixing ratios of these isotopes continue to their neighbors on the chart of nuclides.

The work at Vanderbilt University and Lawrence Berkeley National Laboratory is supported by the U.S. Department of Energy under Grant No. DE-FG05-88ER40407 and Contract No. DE-AC03-76SF00098. The work at Tsinghua University was supported by the National Natural Science Foundation of China under Grant No. 1175095. The work at JINR was partly supported by the Russian Foundation for Basic Research Grant No. 08-02-00089 and by the INTAS Grant No. 2003-51-4496.

References

1. A. Bohr, B.R. Mottelson, *Nuclear Structure*, Vol. **II** (W. A. Benjamin Inc., New York, 1975).
2. C. Goodin, PhD Thesis, Vanderbilt University (2010).
3. K. Krane, R. Steffen, Phys. Rev. C **2**, 724 (1970).
4. K. Krane, Phys. Rev. C **8**, 1494 (1973).
5. W. Greiner, Nucl. Phys. **80**, 417 (1966).
6. S.G. Nilsson, O. Prior, Mat. Fys. Medd. Dan. Vid. Selsk. **32**, 32 (1961).
7. Y.X. Luo, J.O. Rasmussen, A.V. Ramayya, J.H. Hamilton, X.Q. Zhang, J.K. Hwang, C.J. Beyer, J. Kormicki, G.M. Ter-Akopian, Yu.Ts. Oganessian *et al.*, Phys. Rev. C **64**, 054306 (2001).
8. H. Frauenfelder, R.M. Steffen, *Angular correlations*, in *Alpha-,Beta- and Gamma-Ray Spectroscopy*, Vol. **II**, edited by K. Siegbahn (North-Holland Publishing Company, Amsterdam, 1965).
9. P. Ekstrom, DELTA, `www.nndc.bnl.gov/nndcscr/ensdf_pgm/analysis/delta`.
10. A.V. Daniel, C. Goodin, K. Li, A.V. Ramayya, N.J. Stone, J.K. Hwang, J.H. Hamilton, J.R. Stone, Y.X. Luo, J.O. Rasmussen *et al.*, Nucl. Instrum. Methods Phys. Res. B **262**, 399 (2007).
11. G.N. Rao, Hyperfine Interact. **26**, 1119 (1985).
12. D. De Frenne, Nucl. Data Sheets **110**, 1745 (2009).
13. J. Blachot, Nucl. Data Sheets **108**, 2035 (2007).
14. D. De Frenne, A. Negret, Nucl. Data Sheets **109**, 943 (2008).
15. J. Blachot, Nucl. Data Sheets **91**, 135 (2000).
16. G. Gürdal, F.G. Kondev, Nucl. Data Sheets **113**, 1315 (2012).
17. S. Lalkovski, F.G. Kondev, Nucl. Data Sheets **124**, 157 (2015).
18. J. Blachot, Nucl. Data Sheets **113**, 515 (2012).
19. J. Blachot, Nucl. Data Sheets **111**, 717 (2010).
20. S.K. Chamoli, A.E. Stuchbery, S. Frauendorf, J. Sun, Y. Gu, R.F. Leslie, P.T. Moore, A. Wakhle, M.C. East, T. Kibedi, A.N. Wilson, Phys. Rev. C **83**, 054318 (2011).
21. A.G. Smith, D. Patel, G.S. Simpson, R.M. Wall, J.F. Smith, O.J. Onakanmi, I. Ahmad, J.P. Greene, M.P. Carpenter, T. Lauritsen *et al.*, Phys. Lett. B **591**, 55 (2004).
22. A.G. Smith, R. Orlandi, D. Patel, G.S. Simpson, R.M. Wall, J.F. Smith, O.J. Onakanmi, I. Ahmad, J.P. Greene, M.P. Carpenter *et al.*, J. Phys. G: Nucl. Part. Phys. **31**, S1433 (2005).
23. Y.Y. Yang, S.J. Zhu, J.H. Hamilton, A.V. Ramayya, J.K. Hwang, J.O. Rasmussen, Y.X. Luo, K. Li, H.B. Ding, J.G. Wang *et al.*, Chin. Phys. C **33**, S1 (2009).
24. E.F. Jones, P.M. Gore, S.J. Zhu, J.H. Hamilton, A.V. Ramayya, J.K. Hwang, R.Q. Xu, L.M. Yang, K. Li, Z. Jiang *et al.*, Phys. At. Nucl. **69**, 1198 (2006).
25. H.B. Ding, S.J. Zhu, J.H. Hamilton, A.V. Ramayya, J.K. Hwang, Y.X. Luo, J.O. Rasmussen, I.Y. Lee, X.L. Che, J.G. Wang, Chin. Phys. Lett. **24**, 6 (2007).
26. Y.X. Luo, S.J. Zhu, J.H. Hamilton, A.V. Ramayya, C. Goodin, K. Li, X.L. Che, J.K. Hwang, I.Y. Lee, Z. Jiang *et al.*, Int. J. Mod. Phys. E **18**, 1697 (2009).
27. S.J. Zhu, Y.X. Luo, J.H. Hamilton, A.V. Ramayya, X.L. Che, Z. Jiang, J.K. Hwang, J.L. Wood, M.A. Stoyer, R. Donangelo *et al.*, Int. J. Mod. Phys. E **18**, 1717 (2009).
28. Y.X. Luo, J.O. Rasmussen, J.H. Hamilton, A.V. Ramayya, S. Frauendorf, J.K. Hwang, N.J. Stone, S.J. Zhu, N.T. Brewer, E. Wang *et al.*, Nucl. Phys. A **919**, 67 (2013).